Available online at www.sciencedirect.com
SCIENCE DIRECT
Geochimica et Cosmochimica Acta 70 (2006) 1215–1230
Geochimica
www.elsevier.com/locate/gca

The effect of compression on noble gas solubility in silicate melts and consequences for degassing at mid-ocean ridges

Bertrand Guillot [a,*], Philippe Sarda [b,1]

[a] Laboratoire de Physique Théorique de la Matière Condensée, Université Pierre et Marie Curie, UMR CNRS 7600, 4 place Jussieu, 75252 Paris Cedex 05, France

[b] Groupe Géochimie des Gaz Rares, Département des Sciences de la Terre, Université Paris Sud, UMR CNRS 8148 (IDES), 91405 Orsay Cedex, France

Received 2 May 2005; accepted in revised form 2 November 2005

Abstract

The effect of compression on noble gas solubility in silicate melts is still badly understood due to a lack of theoretical guidance. In the experimental literature, noble gases dissolving in liquid silicates are found to concentrate almost linearly with increasing pressure up to several tens of kbar, suggesting that Henry's law could be valid up to very high pressures, although this law stipulates that the gaseous phase in contact with the liquid must be ideal. Recently, new experiments dealing with the dissolution of argon in synthetic and natural silicate melts have pointed out that the evolution of concentration with pressure exhibits a departure from linearity in the 50–100 kbar range, leading either to a levelling off or to a sudden collapse of the argon concentration above 50 kbar. Here, we investigate by means of liquid state physics how volatile species dissolve into silicate melts under pressure. We use a hard sphere model (the reference fluid in liquid state physics) to describe silicate melts and gas at high pressures. One of our main results is that, when pressure increases, the concurrent compaction of gas and melt explains the almost-linear behaviour of the noble gas concentration up to several tens of kbars, before melt compaction dominates and concentration either levels off or decreases gradually in the 50–100 kbar range. In spite of the existence of a quasi-linear regime over a large pressure range, our work disqualifies the use of the Henry law when dealing with high pressures. The implication of these findings to provide an understanding of degassing at mid-ocean ridges is next investigated. Applying our model to the scenario where CO_2 vesicle generation occurs in the magma at mantle depths during its ascent from melting regions, we evaluate magma vesicularity as well as noble gas concentrations in the basalt melt and in vesicles as a function of pressure at depth. It is stressed that the variable and usually strong noble gas elemental fractionation observed in mid-ocean ridge basalts can be explained by assuming a sequence of several vesiculation stages interrupted by vesicle loss during magma ascent.

1. Introduction

The accurate knowledge and understanding of noble gas solubility in silicate melts at depth are of key importance to decipher the degassing history of the Earth mantle. The elemental fractionation in mid-ocean ridge basalts (MORB), if properly interpreted, is believed to give some clues to the main mechanisms leading to degassing of the upper mantle. When basaltic magmas rise under ridges, the most abundant volatile, CO_2, tends to exsolve, forming vesicles. In using a mass balance equation for a closed system, Jambon et al. (1986) showed that the partitioning of noble gases between melt and vesicles depends on noble gas solubility in melt and vesicularity at once. However, the great many data on noble gas concentrations in MORB are difficult to interpret because of the broad variability of the measured values (for instance the $^4He/^{40}Ar$ ratio extends from ~1 to values greater than 100, see Honda and Patterson, 1999). To explain these data, different scenarios have been proposed in the literature (we will not discuss here the possible contaminations of atmospheric or crustal origin). For one of these scenarios (Aubaud et al., 2004), the high elemental fractionations observed in some MORB

* Corresponding author. Fax: +33 1 44 27 51 00.
E-mail address: guillot@lptl.jussieu.fr (B. Guillot).
[1] Present address: Laboratoire de Sciences de la Terre, Ecole Normale Supérieure de Lyon, UMR CNRS 5570, 69364 Lyon Cedex 07, France.

0016-7037/$ - see front matter © 2005 Elsevier Inc. All rights reserved.
doi:10.1016/j.gca.2005.11.007

samples and their supersaturation in CO_2 are explained by a kinetic disequilibrium between He atoms rapidly diffusing into vesicles and more slowly diffusing Ar atoms and CO_2 molecules, when the magma, on transfer from a magmatic chamber, vesiculates at shallow depth under the sea floor. Correlatively, this scenario assumes that the fractionation at depth (i.e., below the magmatic chamber) is governed by the noble gas solubility measured in the laboratory at low pressure. In another scenario (Burnard, 2001), a Rayleigh distillation is invoked to explain the high elemental fractionation (vesicles are assumed to be continuously extracted from the melt during magma ascent, a very restricting scenario), but here also, noble gas solubility data at atmospheric pressure are implicitly assumed to be valid at depth. Very recently, it has been argued (Burnard, 2004) that during mantle melting a preferential enrichment in light atoms (He) with respect to heavier atoms (Ar, Xe) may occur as a consequence of an easier migration of the former ones from solid to melt. Therefore, this enrichment mechanism superimposes to the degassing trajectory of the uprising magma and some caution is recommended in interpreting MORB data. Finally, in an alternative scenario to the Rayleigh distillation, which predicts a much too high $^4He/^{40}Ar$ ratio for MORBs, Sarda and Moreira (2002) pointed out that the tendency of the data points to be distributed around a straight line in a, e.g., $Ln(^4He/^{40}Ar)$ versus $Ln(^{40}Ar)$ diagram, can be explained if several stages of vesiculation are involved, with partial or complete loss of vesicles between the vesiculation episodes, but provided that some pressure effect on noble gas solubilities, not elucidated at that time, is accounted for.

A pressure effect is not unexpected if CO_2 vesicle generation likely occurs at mantle depths in the neighbourhood of melting regions (Bottinga and Javoy, 1990). Hence, the appropriate noble gas solubilities may be different from those measured at atmospheric pressure in the laboratory. Although several authors have tackled this question by experimental means, the conclusion is still unclear. Argon dissolved in silicate melts was found to increase almost linearly with increasing pressure up to several tens of kbar, suggesting that Henry's law would be valid even at these very high pressures. This is very surprising since the simplest form of the Henry law valid at very low pressure assumes that the gas phase is ideal and the Henry's constant independent of pressure. At kbar pressures and above, the gaseous phase is certainly non-ideal and indeed thermodynamics predicts a strong exponential increase of the noble gas concentration in melt and not a linear one, as long as the Henry constant is assumed pressure independent. In recent years, some experimentalists saw a sudden collapse of dissolved argon in various silicate melts at about 50 kbar (Chamorro-Perez et al., 1996, 1998) while other authors saw instead a deviation from linearity and a progressive saturation in argon concentration at around 100 kbar (Schmidt and Keppler, 2002). These conflicting results were interpreted within the framework of the ionic porosity model initiated by Doremus (1966) and popularized more recently by Carroll and Stolper (1993). In this model, the rare gas solubility is related to the concentration in melt of holes (or free volume), which are able to accommodate atoms of a given size. A further scrutiny at solubility data in various silicate melts (Shibata et al., 1998) indicates that noble gas solubility is primarily governed by the free volume induced by network forming ions (the more silicic the melt, the higher the solubility). The model predicts a Henrian solubility behaviour with pressure as long as the available sites are not filled, and a plateau value when all sites are occupied, a global behaviour in agreement with the experimental findings of Schmidt and Keppler (2002). If the hole size distribution is assumed pressure dependent (an increase in pressure shifts the distribution maximum towards smaller cavities due to the compaction of melt), then this model can also explain the abrupt drop in argon solubility above 50 kbar observed by Chamorro-Perez et al. (1998).

In this complicated context, the purpose of our work is to investigate the above intricate questions by means of liquid state physics (a brief account was presented by Sarda and Guillot, 2005). We use the hard sphere fluid, the reference fluid of liquid state theory, to describe silicate melt and gas at high pressure (gas is then a supercritical fluid at the temperature involved at depth), and search how volatile species dissolve into melt as a function of the thermodynamic conditions. Our approach is presented in Section 2. It provides a clear understanding of published high-pressure experiments and emphasizes the role played by the concurrent densification of melt and gas under pressure. In particular, our work explains why experimental results display an almost linear relationship between pressure and noble gas concentration up to several tens of kbars, although it disqualifies the use of the Henry law at these pressures. The implications of the theory for degassing at mid-ocean ridges are discussed in Section 3. A summary of the main results is given in Section 4.

2. Statistical model for the solubility of volatiles in silicate liquids

2.1. Chemical equilibrium

The solubility of a gas in a liquid results from the equality of the chemical potentials of the solute gas in the two phases at equilibrium. For a rare gas fluid in contact with a silicate melt at T and P fixed, the aforementioned equality leads to the relationship,

$$\rho_m/\rho_g = e^{-\beta(\mu_m^{ex}-\mu_g^{ex})} = \gamma_m/\gamma_g, \quad (1)$$

where ρ_m and ρ_g are the number densities (number of particles per unit volume, N/V) of the solute noble gas in the melt and in the gas phase, respectively, $\beta = 1/k_B T$ is the inverse of the temperature with k_B the Boltzmann constant and where μ_m^{ex} and μ_g^{ex} are the excess chemical potentials of the solute in the respective two phases. Coefficient

$\gamma_i = e^{-\beta\mu_i^{ex}}$ (with i = m or g) is the solubility parameter of the rare gas in the corresponding phase. In an experiment, the quantity actually measured is the mole fraction, $X = \rho_m/(\rho_m + \rho_s)$, of noble gas in the solvent melt of number density ρ_s (the number of atoms by unit volume of melt), or alternatively the weight fraction $w_m/(w_m + w_s)$, where w_m is the weight of solute in the melt and w_s the weight of melt. Using Eq. (1), the mole fraction of noble gas in the melt writes

$$X = L/(1+L), \quad \text{where } L = \rho_g\gamma_m/\rho_s\gamma_g. \tag{2}$$

The above equation is quite general and is not restricted to low pressure (notice that generally $L \ll 1$ and $X \sim L$). At very low pressure only, the gas phase can be considered as nearly ideal (i.e., $\gamma_g \approx 1$ and $P_g \approx \rho_g k_B T$) and the mole fraction can be approximated by the well-known Henry's relation

$$X \approx P_g S, \tag{3}$$

where $S = \gamma_m/\rho_s k_B T$ is the solubility constant (the inverse of the Henry constant) expressed in bar^{-1}. Notice that this relation holds as long as the vapour pressure of the melt is sufficiently low for the gaseous mixture (solute gas + silicate vapour) to be considered as ideal. In practice, the solubility constant S is between 10^{-6} and 10^{-8} bar^{-1} for noble gases in MORB at one bar (Kirsten, 1968; Hayatsu and Waboso, 1985; Jambon et al., 1986; Lux, 1987) and, correspondingly, γ_m is between 10^{-2} and 10^{-4}. When pressure increases, the imperfection of the solute gas in contact with melt is accounted for by ρ_g and γ_g in Eq. (2), and expression (3) is no longer valid. However, a common approximation of the literature consists to substitute fugacity, $f = P_g e^{+\beta\mu_g^{ex}}$, to pressure P_g in expression (3). In fact, this procedure is misleading because the relation between P_g and ρ_g is then not correctly accounted for. We will see, later on, that relation (3) holds accurately as long as the density of the gas phase (ρ_g) is very low with respect to that of melt (ρ_s). In contrast, at high pressure, in the kbar range and above, neither the pressure dependence of γ_m and γ_g resulting from the compaction of melt and from the compression of the gas phase, nor the variation of the densities of the two phases, can be neglected when evaluating the noble gas concentration from Eq. (2).

2.2. Equation of state for hard spheres

An effective way to proceed is to evaluate the noble gas concentration X in the framework of the hard sphere (HS) fluid, the reference model in liquid state theory (Andersen et al., 1971). In this model fluid, the atoms (or molecules) are described by hard spheres of diameter d, and the equation of state (EOS) is given with a high accuracy by the Carnahan–Starling equation (Carnahan and Starling, 1969)

$$P = \rho k_B T \frac{1+\eta+\eta^2-\eta^3}{(1-\eta)^3}, \tag{4}$$

while the excess chemical potential of the fluid writes

$$\mu^{ex} = k_B T \frac{8\eta - 9\eta^2 + 3\eta^3}{(1-\eta)^3}, \tag{5}$$

where $\eta = \pi\rho d^3/6$ is called the packing fraction and ρ is the number density (N/V) of the fluid (ρ can vary between nearly zero for the ideal gas to solid-like density when the particles are closely packed). The success of this model to describe real fluids comes from its ability to treat with accuracy excluded volume effects, which predominate over attractive forces when compressing a dense fluid or a liquid. Although the HS fluid has no liquid–gas transition (its structure depends only on the fluid density, not on temperature), one can show that it reproduces very well the EOS of simple gases (noble gases and non polar molecular gases like CO_2) over a large pressure range in the one-fluid region (i.e., at supercritical temperatures). In the present context, this point is important if one remembers that the solubility measurements of volatile species in silicate melts are performed at supercritical conditions for the solute gases ($T_{exp} \sim 1500$–2000 K as compared with $T_c = 150.9$ K for argon, 289.7 K for xenon and 304.2 K for CO_2). For illustration, the pressure-density relation for the isotherm 1600 K is presented in Fig. 1 for He, Ne, Ar, Xe, and CO_2, respectively. In the case of Ne, Ar, and Xe, the fits obtained with Eq. (4) were found almost undistinguishable from the data produced by the EOS of Song and Mason (1989), one of the most reliable EOS for rare gases. For He, which is poorly known experimentally in this (P,T) range, the fit presented here is the one corresponding to a Lennard–Jones fluid (with $\varepsilon/k = 10.22$ and $\sigma = 2.556$ Å, Hirschfelder et al., 1967), while for CO_2 our fit is in agreement with the accurate EOS of Pitzer and Sterner (1994). To be complete, notice that, to reproduce accurately the evolution of compressibility with temperature along an isobar (especially beyond the kbar range), it can be necessary to use a (slight) temperature-dependent hard sphere diameter, $d(T)$, to mimic the tendency of real molecules to interpenetrate more closely during collisions when increasing temperature.

Curiously enough, the compressibility of silicate melts can also be described by the EOS for hard spheres. However, to account for the cohesion energy of the liquid phase, it is necessary, in addition to adjust the hard sphere diameter, to scale the EOS to a reference data point of the real material. A convenient choice is to fit the density of the silicate melt at 1 bar for the temperature investigated experimentally, a density value which is evaluated from the weighted sum of partial molar volumes for the constituent oxides as given in the literature (Bottinga et al., 1983; Lange and Carmichael, 1987). In Fig. 1 are presented the results of such fits for silica at 2000 K, for a MORB at 2000 K and for a San Carlos olivine at 2300 K, respectively. Concerning the olivine melt, our adjustment is based upon the static compression data on liquid peridotite and liquid komatiite obtained by Agee and Walker (1988, 1993) in the range 0–100 kbar. An important finding of these authors is that the bulk modulus (the inverse of the compressibility at one bar)

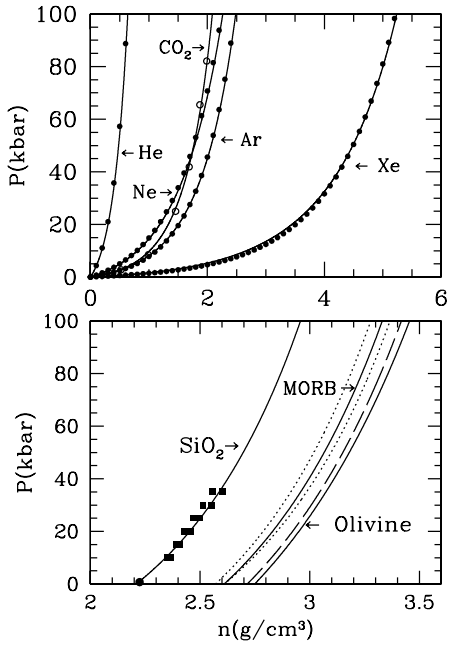

Fig. 1. Pressure (in kbar) versus density (in g/cm^3) for noble gases and various silicate melts using the Carnahan–Starling equation of state. In top panel, the full curves are our evaluations, the black dots are the experimental data points produced by the accurate EOS of Song and Mason (1989) for noble gases and the circles are those for CO_2 as given by the EOS of Pitzer and Sterner (1994). In bottom panel, the full curve labeled SiO2 is our calculation for liquid silica at 2000 K, while the squares represent the data (with error bars) of Gaetani et al. (1998) for the evolution of the density of melt between 10 and 35 kbar and the black dot is the value of the density at one atmosphere as evaluated by Lange and Carmichael (1987). For the MORB, the full curve is our evaluation at 2000 K (see text) and the two dotted curves are the isotherms (1673 and 2000 K) bracketing shock wave compression data of Rigden et al. (1988) for an average MORB. Indeed, along the Hugoniot investigated by Rigden et al. (1988), the temperature increases from 1673 K at atmospheric pressure up to 2000 K at about 100 kbar (see text). For the olivine melt, the full curve is our prediction at 2300 K and the dashed curve is the isothermal compressibility of liquid komatiite at 2200 K obtained by Agee and Walker (1988, 1993). Notice that the shift between theoretical predictions and data comes from the difference in composition between the corresponding melts.

in the liquid phase is found essentially invariant (~260–300 kbar) with composition in these magnesian silicates, a finding that we can assume also true for the olivine melt whose composition is very close. Our EOS leads to very good fits of the data for peridotite and komatiite melts (Agee and Walker (1988, 1993)) simply by imposing the melt composition and the value of the bulk modulus at one bar. Then, noticing that the San Carlos olivine melt has a density at atmospheric pressure slightly higher than that of a komatiite and a peridotite (2.82 g/cm^3 at 2000 K as compared with 2.72 for a komatiite and 2.76 for a peridotite, after Lange and Carmichael, 1987), we can predict the variation of its density with pressure (see Fig. 1 for an illustration). In the case of the MORB investigated here (that of Jambon et al., 1986), we used the shock wave compression data that Rigden et al. (1984, 1988) have obtained from an average MORB. However, in a shock wave experiment the temperature is not constant along the Hugoniot and, in the present case, the authors have estimated that the temperature increases from 1673 to roughly 2000 K when the pressure evolves from atmospheric pressure to 100 kbar. From these findings, and with the help of our EOS, we have evaluated the two isothermal compressibility curves (1673 and 2000 K) delimiting the Hugoniot reported by Rigden et al. (1984, 1988) in the pressure range 0–100 kbar: theses curves are reported in Fig. 1 as dotted lines. The EOS is then deduced simply from the previous curves in noticing that our MORB is almost identical to the anorthite–diopside mixture investigated by Rigden et al. (1984, 1988), except for a slight increase in density at atmospheric pressure (2.61 g/cm^3 instead of 2.57 g/cm^3 at 2000 K) due to a small difference in composition. As for the Fe-free synthetic tholeiite investigated by Schmidt and Keppler (2002), we have used the same hard sphere diameter than previously with the natural MORB while the reference density at atmospheric pressure was changed according to its specific composition (2.43 g/cm^3 at 2000 K). In the case of silica, we have fitted the volumetric data obtained by Gaetani et al. (1998) for rhyolitic melts at high pressure (10–35 kbar). Notice that our EOS leads to a bulk modulus for silica of about 140 kbar at atmospheric pressure, in agreement with the data of Lange and Carmichael (1987), while at 35 kbar the bulk modulus amounts to 310 kbar, as compared with 303 ± 21 kbar by Gaetani et al. (1998). For the haplogranite melt considered in the present paper, we assume that its bulk modulus is identical to the one of pure silica (which means that the hard sphere diameters are identical for the two melts), but the reference density at 1 bar is modified according to composition (2.25 g/cm^3 for the Fe-free haplogranite instead of 2.22 g/cm^3 for silica at 2000 K).

From a more general point of view, several points merit comments. The uncertainty in the determination of the hard sphere diameter comes mainly from the inaccuracies in the experimental data to fit and very little from the ability of the EOS to interpolate reliable data points (as far as the pressure range under investigation is not too large, i.e., about $0 \sim 100$ kbar). Thus, an experimental uncertainty of about $\pm 10\%$ on pressure (the order of magnitude of the uncertainties in the data considered above) leads to an uncertainty of about $\pm 1\%$ on the hard sphere diameter of the corresponding melt. Concerning the dependence of the latter on composition, we observe a decrease of diameter when going from highly silicic melts (e.g., $d \sim 3.27$ Å for silica and rhyolitic melts) to ultrabasic melts (e.g., $d = 2.82$ Å for olivine melt). More precisely, d decreases almost linearly with the concentration in magnesium oxide (not shown). Another important correlation is that the reduced density, $\rho^* = \rho d^3$ (where ρ is the numerical density (N/V) of the melt at atmospheric pressure and d the corresponding hard sphere diameter), is remarkably constant whatever the composition of melt ($\rho^* = 0.803 \pm 0.025$ when considering silica, MORBs, peridotite, komatiite and olivine

melts), which enables to predict a priori the hard sphere diameter for any melt with a good accuracy.

From the fits obtained above for rare gases, CO_2 and silicate melts, it is easy to deduce the respective densities at equilibrium for gas (ρ_g) and melt (ρ_s) when both phases are in contact with each other at fixed T and P. In the following, we will neglect the slight modification experienced by melt due to the incorporation of a very weak concentration of solute gas ($X \ll 1$), and, in the same way, we will neglect the influence on the fluid phase of the silicate vapour escaping from melt.

2.3. Solution of noble gases into silicate melts

To evaluate concentration X from the Eq. (2), it remains to calculate the solubility parameters γ_m and γ_g. The latter one is obtained from Eq. (5) for a pure rare gas fluid and γ_m is evaluated according to the scaled particle theory developed for hard spheres in the early sixties (Reiss et al., 1960). In this theory, the excess chemical potential of a hard sphere solute (considered at infinite dilution) in a hard sphere solvent is nothing but the work of creating a spherical cavity of desired size in the solvent, a purely entropic contribution given by

$$\mu_{cav}^{ex}/k_BT = -\ln(1-\eta) + \frac{6\eta}{1-\eta}(-\lambda + 2\lambda^2) + \frac{18\eta^2}{(1-\eta)^2}\left(\frac{1}{4} - \lambda + \lambda^2\right) - \eta\frac{1+\eta+\eta^2-\eta^3}{(1-\eta)^3}(1 - 6\lambda + 12\lambda^2 - 8\lambda^3), \quad (6)$$

where $\eta = \pi\rho d^3/6$ is the packing fraction in the solvent of hard sphere diameter d and number density $\rho = N/V$, and $\lambda d = (d_i + d)/2$ is the radius of the cavity enclosing the solute particle of diameter d_i. This expression is virtually exact for hard spheres (Attard, 1993) and has been very useful to interpret gas solubility data in molecular and complex liquids (Pierotti, 1976; Kodaka, 2001). An immediate and important information given by Eq. (6) is that, for a given melt, the larger the noble gas to absorb, the higher the entropy cost of cavity formation and the smaller the resulting solubility. In the same way, for a given solute, the denser the silicate, the higher the entropy cost and the lower the probability of insertion, $e^{-\beta\mu_{cav}^{ex}}$. So, at this stage, our theory predicts that xenon is less soluble than helium and that highly silicic melts have more affinity for noble gases than ultrabasic melts do (a result in agreement with the finding of Shibata et al. (1998), who stressed the role played by network forming ions to the noble gas solubility). However, there is no solvation energy in a hard sphere fluid, only the entropic contribution given above. So, the energetic contribution to the excess chemical potential has to be evaluated from another footing and added to the entropic contribution (given by Eq. (5) for a pure fluid and by Eq. (6) for a solute diluted in a solvent). Although the energetic contribution is small in compressed rare gas fluids and in non-polar gases at supercritical conditions (as investigated here), this is not true for noble gases in a silicate melt. It has been shown (Guillot and Guissani, 1996a) that the dominant contribution to the noble gas solvation energy is the charge-induced dipole interaction resulting from the polarization of the rare gas atom by the Coulomb field created by the ionic species of the silicate melt, namely

$$E_{pol} = -\tfrac{1}{2}\alpha_X\langle F^2\rangle, \quad (7)$$

where α_X is the polarizability of the solute, F is the Coulomb field polarizing the solute and $\langle\rangle$ expresses a canonical averaging over all the configurations of the melt. This polarization energy is attractive and is expected to be small for a weakly polarizable atom such as helium ($\alpha_{He} = 0.2\ A^3$) and much more significant for xenon ($\alpha_{Xe} = 4.0\ A^3$). A key point is that $\langle F^2\rangle$ is a quantity depending strongly on the distribution of ionic species in the melt. In other words, its value depends on the nature and the structure of the silicate melt under investigation. Furthermore, due to the $(1/r)$ dependence of the Coulomb potential, $\langle F^2\rangle$ is a slowly varying function of the interionic distances in the melt and consequently, because of the weak compressibility of silicate melts, it depends very little on external pressure (in contrast to the entropy of cavity formation (Eq. (6)), which varies drastically with the density of melt because it is a local property). Unfortunately, it is not possible to evaluate analytically from first principles the solute polarization energy in a system as complicated as a silicate melt. This can be done only by computer simulation and it is a task far beyond the scope of this study (however, for noble gases in simulated silica, see Guillot and Guissani, 1996a).

Thus, in practice, we have checked that the solubility constants ($S = \gamma_m/\rho_s k_B T$) of noble gases in various silicate melts can be quantitatively reproduced in putting

$$\mu_m^{ex} = \mu_{cav}^{ex} + E_{pol}, \quad (8)$$

where E_{pol} is treated as a fitting parameter and μ_{cav}^{ex} is calculated from Eq. (6) (notice that the hard sphere diameters $d(T)$ and $d_i(T)$ entering into expression (6) for μ_{cav}^{ex}, were adjusted previously to reproduce the EOS of the silicate melt and that of the rare gas fluid under investigation). For illustration, we present in Fig. 2 the decomposition of μ_m^{ex} into its two contributions for noble gases and CO_2 in rhyolite (Carroll and Stolper, 1993), in MORB (Jambon et al., 1986) and in komatiite (Carroll and Draper, 1994), as constrained from the solubility constants (or Henry's constant) of the literature. We have also evaluated noble gas solubilities in enstatite (investigated by Kirsten, 1968, and Shibata et al., 1998), but the results are very close to those in komatiite and for this reason are not reported in the figure. It is clear from Fig. 2 that the denser the silicate, the larger the entropic contribution to the chemical potential (thus, the denser the melt, the lower the probability to accommodate an atom of a given size). As for the polarization energy, it contributes very little, as expected, to the

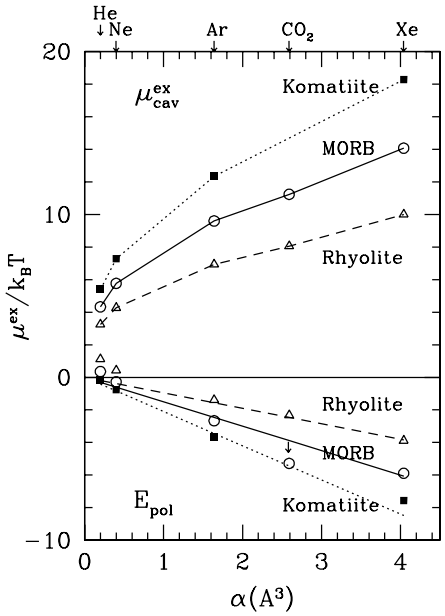

Fig. 2. Entropic (μ^{ex}_{cav}) and energetic (E_{pol}) contributions to the excess chemical potential of noble gases and CO_2 in various silicate melts at 1673 K and 1 bar. Notice that only the entopic term (μ^{ex}_{cav}) is evaluated explicitly by the theory (see text), the polarization energy being obtained from the difference ($\mu^{ex} - \mu^{ex}_{cav}$), where μ^{ex} deduced from solubility data of the literature (see the definition of S in Eq. (3)). One sees that the entropy penalty increases strongly with the size of the rare gas while the solvation energy decreases almost linearly with the polarizability of the atom (or molecule) as stipulated by the theory (see text). In the case of CO_2 in MORB, the polarization energy deviates significantly from the expected linear behavior (see the arrow) because of the occurrence of carbonate ions which interact strongly with the melt through coulombic forces. In rhyolite, CO_2 behaves like a rare gas, a finding in agreement with literature data, which report its molecular character when solvated in highly silicic melts.

chemical potential of helium and neon whatever the silicate, while it contributes significantly to that of argon and xenon, but not to the point to overcompensate the entropic term as it happens with the noble gases in water, for instance (see Guillot and Guissani, 1996a). Considering the experimental uncertainties, the proportionality of E_{pol} with noble gas polarizability (see Eq. (7) and Fig. 2) is well supported by the data. Nevertheless, one notices a slight but systematic deviation from linearity exhibited by helium (and to a lesser extent by neon), which suggests that the helium solubility could be underestimated (up to a factor of 2) in experiments, due to its high diffusivity. Another important information is that the magnitude of the polarization energy follows the hierarchy rhyolite < MORB < komatiite. This finding can be rationalized in pointing out that the total polarizing field F acting on the solute is the result of a summation over all the individual fields emanating from the ionic species forming the silicate. In pure silica melt, it has been established both by simulation (Guillot and Guissani, 1996a) and by X-ray scattering (Wulf et al., 1999) that the noble gases occupy, in the silica network, the center of a cage (clathrate-like) of rather high symmetry and hence the Coulomb field felt by the rare gas atom is cancelled to a large extent, the net result being a weak polarization energy. This explains why the noble gases, in a highly silicic melt as rhyolite, exhibit a much smaller polarization energy than in a less polymerized melt like a MORB. A further interesting finding concerns CO_2, which is known to be dissolved preferentially as a molecular species in rhyolite (Fogel and Rutherford, 1990; Tamic et al., 2001) and under the form of a carbonate ion in MORB (Fine and Stolper, 1985). Thus, it is striking on Fig. 2 that CO_2 in rhyolite behaves as a molecular species whose polarizability is intermediate between that of Ar and Xe, while in MORB the associated polarization energy is significantly lower than expected from the linear law, which indicates that CO_2 is certainly more ionic (carbonate ion) than molecular when dissolved in a basalt.

2.4. Pressure dependence of noble gas solubility in silicate melts

Coming back to our goal of evaluating the concentration of a volatile species in a silicate melt, we first discuss the evolution with pressure of the solubility parameters γ_m and γ_g. The density dependence of the latter quantity is given by Eq. (5) for the pure fluid whereas that of γ_m is governed by the entropic term μ^{ex}_{cav} figuring in Eq. (8) and detailed in Eq. (6) (the polarization energy being assumed invariant with pressure and estimated from a fit of the solubility data at very low pressure, as discussed earlier). For illustration, is shown in Fig. 3 the evolution with pressure of the solubility parameters γ_m and γ_g of He, Ne, Ar, and Xe in a representative MORB (Jambon et al., 1986) along the isotherm 1673 K. It is clear that, as soon as the kbar range is reached, neither the compaction of melt nor that of the rare gas fluid can be neglected. Indeed, both γ_m and γ_g decrease by several orders of magnitude between 1 and 100 kbar, the larger the rare gas the stronger the decrease. These findings are at variance with the common assumption that the Henry's constant ($K_H^{-1} \propto \gamma_m$) is invariant when increasing pressure and that the rare gas fluid can be considered as ideal (i.e., $\gamma_g \approx 1$). More surprising is the behaviour of the ratio (γ_m/γ_g) which mainly governs the evolution of concentration X (see Eq. (2)). This ratio increases with pressure and tends to saturate for He and Ne above 100 kbar, while it goes through a maximum for Ar and Xe around 70–90 kbar. This means that, over a large pressure range, the affinity of a noble gas for the melt increases with pressure while that for its parent fluid decreases! The role played by the concurrent densification of the two phases sheds a new light on the behaviour of noble gases in silicate melts under pressure.

2.5. Effect of the several parameters on concentration

In Fig. 4 are shown diagrams of noble gas concentration versus pressure, calculated from Eq. (2). Our calculation agrees with the common observation of the literature

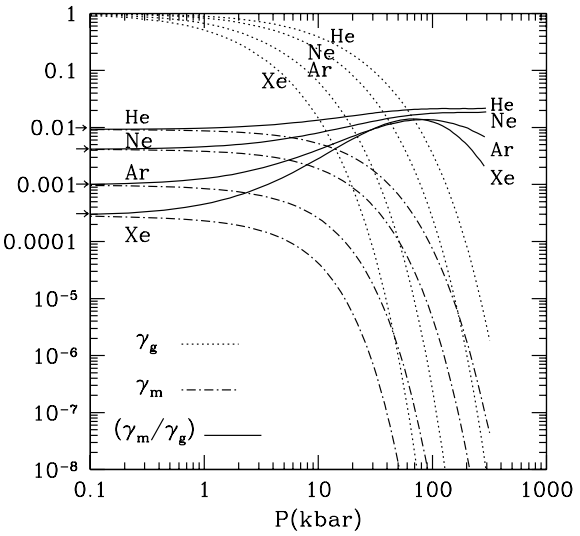

Fig. 3. Calculated solubility parameters of noble gases in a tholeiitic melt at 1673 K as a function of pressure. The basalt composition is the same as the one investigated by Jambon et al. (1986), its density at one bar was deduced from its chemical composition using the partial molar volumes of oxide components (Bottinga et al., 1983). The diameter of the hard sphere describing the basalt ($d = 3.18$ Å) was deduced by fitting high-pressure data on basaltic melts (see Fig. 1). The hard sphere diameters of the noble gases ($d = 1.86$ Å, $d = 2.21$ Å, $d = 2.91$ Å, and $d = 3.515$ Å) were deduced from fits of their (PVT) data using the EOS for hard spheres, as shown in Fig. 1. The arrows indicate the value of the solubility parameter γ_m of the noble gases in melt at one atmosphere, which corresponds to the solubility constant S measured by Jambon et al. (1986). Henry's law would correspond to horizontal lines.

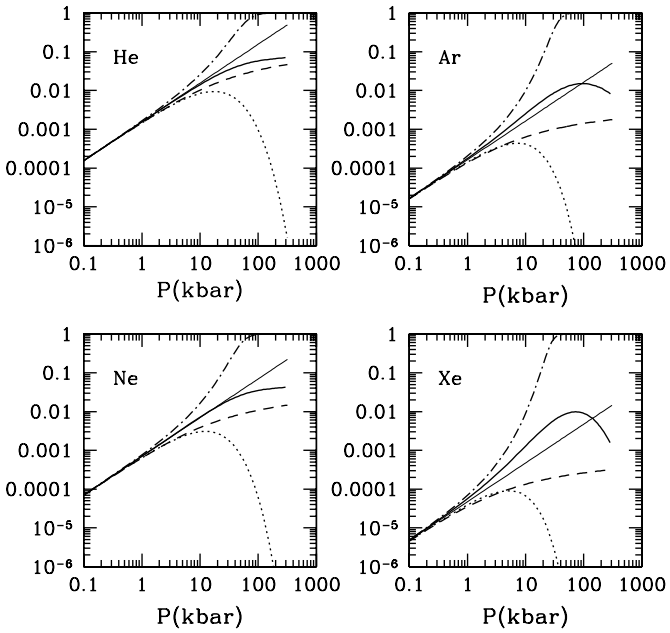

Fig. 4. Concentrations (in mole fraction) of He, Ne, Ar, and Xe in a tholeiitic melt at 1673 K as function of pressure. The straight line represents Henry's law, the dashed curve characterizes the deviation from Henry's law when only the variation of the density of the fluid with pressure is taken into account (see text), the dotted-dashed curve is the result when the imperfection of the gas is accounted for in γ_g, the dotted curve when the gas phase is assumed ideal while introducing the melt compaction through the variation with pressure of γ_m and ρ_s neglected up to now (see text and Eq. (2)), and the bold curve is the correct behavior when all the contributions are put together.

(White et al., 1989; Carroll and Stolper, 1993) that the concentration of noble gases increases almost linearly with pressure, as stipulated by the Henry law, even in the kbar range and above (see bold curves and compare with the thin lines based upon the solubility data at 1 bar (Jambon et al., 1986)). However, at higher pressure, when the deviation from linearity becomes obvious, it depends on the rare gas under investigation. For helium, and to a lesser extent for neon, the deviation from Henry's law occurs downwards, the concentration tending to saturate beyond 100 kbar. For argon and xenon the deviation occurs first upwards, then the concentration curve bends and goes through a maximum around 70–90 kbar just before crossing the Henry line. This complex behaviour is the result of a subtle balancing between the quantities entering into the definition (2) of X. For instance, assuming in Eq. (2) that γ_m is constant and $\gamma_g = 1$ (i.e., that Henry's law holds), the simple introduction into Eq. (2) of the true variation of the noble gas density ρ_g with pressure improves qualitatively the results with respect to Henry's law (see dashed curves in Fig. 4). If, in addition, the imperfection of gas is implemented into γ_g (see Eq. (2)), not only one obtains no improvement but the concentration increases much too rapidly when pressure reaches the kbar range (see dashed-dotted curves). In contrast, if one neglects the non-ideality of the gas phase (then $\gamma_g = 1$ is restored) while introducing the variation with pressure of γ_m and ρ_s (melt compaction) neglected up to now, this approximation leads to a rapid drop of the noble gas concentration above 10 kbar (see dotted curves). So, the correct evolution of the concentration with pressure expresses the antagonism between the increasing difficulty for the rare gas to stay in its parent fluid under pressure and its decreasing probability to penetrate the compacted melt. In summary, although the Henry law seems to provide a rather good extrapolation for the noble gas concentration data in the kbar range (and even above for He and Ne), the approximations underlying the law (ideality of the gas phase and invariance with pressure of the noble gas excess chemical potential in melt) are flawed and misleading at such pressures.

2.6. Comparison with experimental data

From the experimental point of view, there exists a number of noble gas solubility data at high pressure in various silicate liquids (White et al., 1989; Montana et al., 1993; Carroll and Stolper, 1993), but the 10–100 kbar range was reached only recently by a few authors. In Fig. 5 are presented the concentration data for Ar in silica and in San Carlos olivine by Chamorro-Perez et al. (1996, 1998) as well as those obtained by Schmidt and Keppler (2002) with Fe-free synthetic haplogranitic and tholeiitic melts.

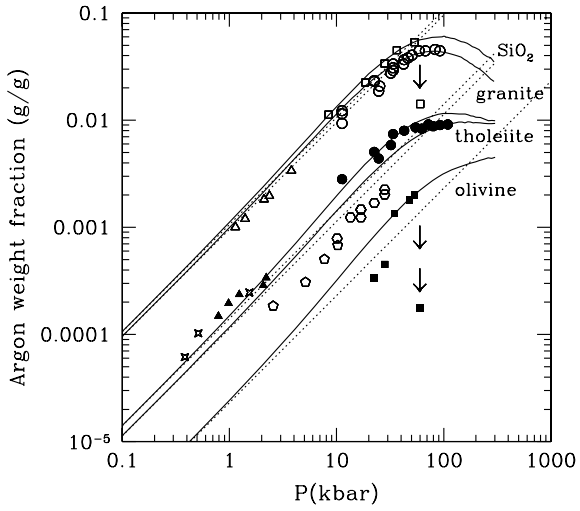

Fig. 5. Calculated argon concentration (weight fraction) for pure argon in contact with silica, haplogranite, tholeiite and olivine melts, as a function of pressure. For silica and haplogranite the calculations were performed at 2000 K, for tholeiite they were performed at 1800 and 2300 K (the lowest curve) because the experimental data covers this temperature range, and for olivine they were performed at 2300 K. The hard sphere diameter of the synthetic haplogranite is assumed identical to that used for silica ($d = 3.27$ Å) in Fig. 1. The hard sphere diameter of the synthetic tholeiite is assumed identical to that used for MORB ($d = 3.18$ Å) in Fig. 1, while the one describing olivine melt ($d = 2.82$ Å) is taken from Fig. 1. The solubility constants for argon at one bar in tholeiite and granite are assumed identical to that measured in MORB (Jambon et al., 1986) and rhyolite (Carroll and Stolper, 1993), respectively, whose values were used to draw Fig. 2. As for the argon solubility constant in silica, our fit of the high pressure data (open squares) of Chamorro-Perez et al. (1996) leads to a value very close to the one reported for silica glass at 1000 °C by Carroll and Stolper (1991), Carroll and Stolper (1993) ($S = 61.8 \times 10^{-5}$ cm^3 STP/g bar instead of 69.1×10^{-5} cm^3 STP/g bar). The empty and solid circles represent the data of Schmidt and Keppler (2002) for their Fe-free synthetic haplogranite and tholeiite, respectively. Are also shown for comparison in the intermediate pressure range (1–25 kbar) some Ar data for rhyolite (empty triangles: Carroll and Stolper, 1993) and natural basalts (full triangles: BU-basalt of Carroll and Stolper, 1993; stars: EMS-basalt of Carroll and Stolper, 1993; pentagons: RE-basalt of Carroll and Stolper, 1993; hexagons: olivine tholeiite of White et al., 1989), whose compositions are close or related to those investigated by Schmidt and Keppler. For natural basaltic melts, one notices that the solubility data of White et al., for an olivine tholeiite and that corresponding to the RE-basalt of Carroll and Stolper (also an olivine tholeiite) are clearly below our tholeiite line, as expected, while those associated with normal basalts (BU- and EMS-basalt) are quite close to it. In the case of the olivine melt, our argon solubility constant ($S = 1.8 \times 10^{-5}$ cm^3 STP/g bar, see the dotted line) adjusted to reproduce at best the high pressure solubility data (closed squares) of Chamorro-Perez et al. (1998) in the 30–45 kbar range is between that measured in enstatite melts (Kirsten, 1968; Shibata et al., 1998) ($S \sim 2.0 \times 10^{-5}$ cm^3 STP/g bar) and the one measured in komatiite (Carroll and Draper, 1994) ($S \sim 1.0 \times 10^{-5}$ cm^3 STP/g bar). Alternatively, a fit of the olivine solubility data in the 10–20 kbar range would lead to a much too small value of S and we discarded these data points. Notice the abrupt drop in Ar concentration (indicated by the arrows) reported by Chamorro-Perez et al. in silica (open squares) and in olivine (closed squares) above 50 kbar.

Concerning the argon concentration data of Schmidt and Keppler (2002), one notices that they are remarkably described by our theoretical curves. (An uncertainty of about ±10% on the pressure leads to an uncertainty in Ar concentration of about ±10% around the maximum of concentration and less than ±1% in the linear region). The same agreement between theory and experiment is also obtained for xenon in synthetic tholeiitic melt (not shown; however, see Fig. 4 for Xe in MORB and compare with Schmidt and Keppler (2002)) although in that case, some adjustment of the solubility constant for xenon is necessary, an adjustment which is not unexpected when considering the large uncertainties in solubility data for this rare gas (see Jambon et al., 1986). For completeness, are also shown, in the 1–25 kbar pressure range, argon data in rhyolite and natural basalts (White et al., 1989; Carroll and Stolper, 1993) whose compositions are close to the synthetic materials investigated by Schmidt and Keppler. The theory predicts the existence of a maximum of concentration in haplogranite around 80 kbar and beyond 100 kbar for the tholeiitic melt, although less pronounced in this case. Notice that the effect of temperature is weak but not negligible (the experimental temperature range is 1800–2300 K: a higher temperature tends to shift the curve to a higher pressure and to flatten the concentration maximum). The levelling off seen in the data was interpreted (Schmidt and Keppler, 2002) as due to a saturation effect whereby the host sites for Ar atoms in the melt structure all become occupied. In contrast, for the present statistical theory, there are no predefined holes in a liquid and it is the density fluctuations which are governing the probability of accommodating a solute of a given size. So, the appearance of a quasi saturation of the noble gas concentration at very high pressures is nothing but the result of a cancellation effect during the concurrent compaction of the two phases (melt and gas).

In the case of olivine, we cannot reproduce the entire data set of Chamorro-Perez et al. (1998) and especially the abrupt decrease of the argon concentration around 50 kbar. However, the value at low pressure of the argon solubility constant in the San Carlos olivine used in our model ($S^{Ar} = 1.8 \times 10^{-5}$ cm^3 STP/g bar, see the dotted line in Fig. 5) is in agreement with that measured in enstatite melts ($\sim 2.0 \times 10^{-5}$ cm^3 STP/g bar see Kirsten, 1968, and Shibata et al., 1998) and in komatiite ($\sim 10^{-5}$ cm^3 STP/g bar see Carroll and Draper, 1994). Besides, the hard sphere diameter associated with the San Carlos olivine was assumed identical to the one determined for komatiite (see Fig. 1). Curiously enough, in another study, Chamorro-Perez et al. (1996) presented data for Ar in silica (see Fig. 5), which also exhibits an abrupt decrease in the same pressure range. These latter data are in contradiction to those of Schmidt and Keppler (2002) for a highly silicic melt (haplogranite), and with our own calculations for silica and haplogranite (see Fig. 5) which predict instead a broad maximum around 80 kbar. One may argue that the dissolution of rare gas atoms into the melt could significantly modify its response to pressure (compressibility) in inducing, for instance, a drastic change of the melt structure above a threshold pressure (a possibility which is not taken into account in the present state of our theory). However, the fact the abrupt decrease of the Ar concentra-

tion is observed almost at the same pressure for two melts of very different composition (e.g., silica and olivine) and for argon concentrations that differ by one order of magnitude from one another, seems to rule out this explanation. In the same way, the few basic and ultrabasic silicate liquids which have been investigated by static and shock-wave compression techniques (Rigden et al., 1984; Agee and Walker, 1988, 1993) do not seem to exhibit anomalies in their EOS below 100 kbar, an observation which does not support an eventual structural change in olivine melt near 50 kbar, except if the presence of the rare gas plays a role in this respect. Another explanation could be the crystallization of the rare gas fluid. But, at 2300 K, argon crystallizes near 350 kbar and xenon around 130 kbar (Boehler et al., 2001), a pressure range not yet reached up to now. So, at this time, our opinion is that the behaviour predicted by the present model and observed by Schmidt and Keppler (2002), namely, the rare gas concentration saturates gradually or goes through a broad maximum with increasing pressure (depending on the melt composition and the noble gas), is essentially correct.

3. Elemental fractionation in MORB

3.1. Noble gas vesicle-melt partitioning

As emphasized in the introduction, one of our goals is to evaluate the implications of the above compression effect on the elemental fractionation of noble gases between vesicles and melt during magma ascent at mid-ocean ridges. When CO_2 exsolves from magma due to the pressure drop induced by ascent (e.g. Bottinga and Javoy, 1990), the dissolved noble gases redistribute between bubbles and melt. The equality of the chemical potentials of one rare gas in the vesiculated magma and in the bubbles of CO_2, considered at equilibrium, leads to the same relation than Eq. (1) except that ρ_g is now the number density of the rare gas in the CO_2 phase and μ_g^{ex} its excess chemical potential (ρ_m still is the number density of the rare gas in melt and μ_m^{ex} the associated excess chemical potential). In addition, for a closed system, the fractionation between vesicles and melt fulfils the simple mass conservation law,

$$C_0^i = C_v^i + C_m^i, \tag{9}$$

where C_0^i (expressed in cm^3 STP/g or in mol/g) is the concentration of rare gas i in the magma before vesiculation, C_v^i the concentration in vesicles and C_m^i the concentration in melt. The introduction into Eq. (9) of the chemical equilibrium conditions discussed above (see Eq. (1)) leads to the following expressions:

$$C_v^i = C_0^i \frac{(\gamma_g^i/\gamma_m^i)V^*}{1 + V^*[(\gamma_g^i/\gamma_m^i) - 1]}, \tag{10}$$

$$C_m^i = C_0^i \frac{1 - V^*}{1 + V^*[(\gamma_g^i/\gamma_m^i) - 1]}, \tag{11}$$

where $V^* = V_g/(V_g + V_m)$ is called vesicularity (V_g is the volume of gas and V_m the volume of melt), and $\gamma_{g,m}^i = e^{-\beta\mu_{g,m}^{i,ex}}$ are the solubility parameters of noble gas i in melt (considered at infinite dilution in the following) or in the CO_2 phase. The above relations are exact at equilibrium whatever pressure is, and they replace the expressions of the literature (Jambon et al., 1986), which are valid only at very low pressure (in this case $\gamma_g^i \approx 1$ and $\gamma_m^i \approx \rho_s k_B T S_i$ where the solubility constant, S_i, is the inverse of the Henry constant). Notice that the simplicity of relations (10) and (11) is only apparent because all the quantities figuring in them must be calculated self-consistently. Thus, vesicularity, V^*, cannot be used as a free parameter but has to be evaluated for the thermodynamic conditions prevailing at depth. This can be done by applying the mass conservation law to the exsolution of CO_2 molecules from melt. If exsolution of CO_2 begins at pressure P_0, then, at any pressure $P < P_0$ during magma ascent (considered as isothermal), vesicularity writes

$$\frac{V^*}{1 - V^*} = \frac{\gamma_m^{CO_2}}{\gamma_g^{CO_2}} \left(\frac{\rho_m^{CO_2}(P_0) \times \rho_s(P)}{\rho_m^{CO_2}(P) \times \rho_s(P_0)} - 1 \right), \tag{12}$$

where $\gamma_m^{CO_2}$ is the solubility parameter of CO_2 in melt at pressure P, $\gamma_g^{CO_2}$ its solubility parameter in the CO_2 phase in equilibrium with the melt, $\rho_m^{CO_2}(P)$ the number density of CO_2 molecules in melt at pressure P, $\rho_m^{CO_2}(P_0)$ the number density at the initial pressure P_0, and ρ_s the number density of melt depending on pressure. If exsolution only occurs when some degree of super-saturation in CO_2 is reached in melt (i.e., when ascent is so rapid that chemical equilibrium cannot be achieved), then the term (-1) on the right hand side of Eq. (12) may be replaced, as a first approximation, by $(-f)$ where $f = N^{CO_2}(P)/N_{eq}^{CO_2}(P)$ expresses the ratio of the number of CO_2 molecules really in the melt to the number expected at saturation.

3.2. Vesiculation during ascent from melting regions

The evaluation of vesicularity by Eq. (12) needs to know the evolution of the CO_2 concentration in the silicate melt with thermodynamic conditions. Applied to the case of CO_2, our solubility model leads to a prediction which interpolates quite accurately (i.e., within the experimental uncertainties) the concentration data of CO_2 in tholeiitic melts over the entire pressure range investigated up to now (Pan et al., 1991; Dixon, 1997). Assuming a solubility constant of 0.44 ppm CO_2/bar (at 1 bar), a conservative value considering the rather large dispersion of the data at low pressure (for a compilation see Jendrzejewski et al., 1997), we obtain 535 ppm at 1 kbar, 0.75 wt% at 10 kbar and 1.6 wt% at 20 kbar as compared with 543 ppm at 1 kbar, 0.77 wt% at 10 kbar and 1.6 wt% at 20 kbar by Pan et al. (1991). Incidentally, our model also predicts a maximum of concentration of about 2.1 wt% near 35 kbar (a feature interesting to verify by experiment, especially in silicic melts like rhyolite, where CO_2 is solvated

preferentially as a molecular species). A more elaborate theory dealing with the solvation of carbon dioxide in molten basalts should describe explicitly the chemical equilibrium between molecular (CO_2) and ionic (CO_3^{2-}) species and its possible pressure dependence. Although we could improve our simple approach along this way (e.g. in Guillot and Guissani, 1996b), this is beyond the scope of this work and, under its present form, our model provides essentially a useful interpolation formula to describe the pressure dependence of the CO_2 solubility in MORB (in fact, the energetic part of the CO_2/CO_3^{2-} transition is taken into account in an effective way by our procedure of adjusting E_{pol}). In addition, carbonate and molecular CO_2 are expected to show significantly different behaviors at pressures above that of the maximum concentration, but it is sufficient for our purpose to describe quantitatively the evolution with pressure of the CO_2 concentration in MORB for depths lower than those at which melting is expected to begin (<100 km or $P < 35$ kbar).

Introducing the evolution of the CO_2 concentration with pressure into Eq. (12) permits us to describe the evolution of V^* in a tholeiitic melt during magma ascent, as illustrated in Fig. 6A for different initial conditions ($P_0 = 1$, 5, 10, 30 kbar and $f = 1$, 4). One notices a rapid evolution of vesicularity with pressure and a rather weak influence of a super-saturation in CO_2 on the vesicularity at eruption

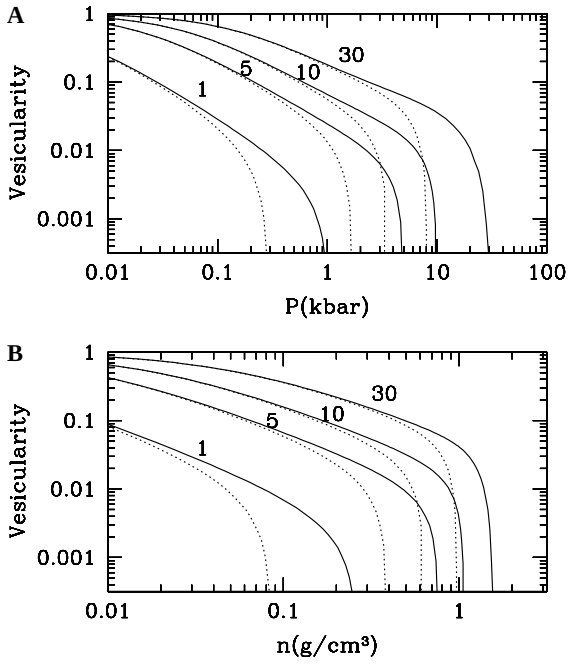

Fig. 6. Evolution of the vesicularity of a MORB with pressure (top panel) and fluid density (bottom panel) during magma ascent. Assuming that vesiculation begins when the pressure in magma equals the saturation pressure of CO_2, four initial conditions are presented, namely $P = 1$, 5, 10, and 30 kbar (full curves). The dotted curves correspond to exsolution beginning only after super-saturation is reached (here 4 times the CO_2 saturation value at P_{sat}). Notice that for $P = 10$ kbar, the vesicularity amounts to 17% for a magma erupting on the ocean floor at 3300 m under sea level, a value in agreement with the vesicularity measured in popping rocks (see text).

on the ocean floor, as long as exsolution begins at a pressure larger than 5 kbar (compare the full curves with the dotted ones in the range 0.3–0.4 kbar, which corresponds to 3000–4000 m under sea level). Obviously, the degree of super-saturation has a strong influence on the depth at which CO_2 exsolution occurs, the greater the super-saturation, the lower the vesiculation pressure. On the other hand, at depth, when vesicularity remains sufficiently low ($V^* < 10^{-2}$), the density of the fluid in the vesicles is high (see Fig. 6B), and is comparable to that of liquid CO_2 at low temperature (the critical parameters of CO_2 are $T_c = 31.1$ °C, $n_c = 0.466$ g/cm^3 and $P_c = 73.8$ bar), a fact not fully appreciated until now. For instance, the ratio of the numerical density of the fluid (the number of particles by volume unit) to that of the melt is as high as 0.5 at 10 kbar.

3.3. Undegassed samples: the popping rocks

Among all MORB tholeiites, the popping rocks are those presenting the largest vesicularity and the largest concentration in CO_2 and other volatiles (Javoy and Pineau, 1991). Moreover, they show a He isotopic ratio similar to the mean MORB ratio ($^4He/^3He \sim 88{,}000$; see Moreira et al., 1998), suggesting that they probe the same mantle source depleted in primordial ^3He. In addition, they have among the lowest known $^4He/^{40}Ar$ ratios for MORB tholeiites, and a regular vesicle-size distribution (Sarda and Graham, 1990). For these reasons, popping rocks are often considered as undegassed basalts from the upper mantle. In contrast, the ocean island basalts (OIB) exhibit a smaller $^4He/^3He$ ratio (for a discussion see Graham, 2002) indicating a less degassed source mantle for OIB than for MORB, namely the lower mantle.

Assuming that popping rocks are undegassed samples representative of the source mantle from which MORBs are generated, we have introduced into Eq. (12), as initial abundance, the CO_2 concentration of 0.75 wt% estimated for the popping rock 2Π*D*43 by Graham and Sarda (1991). This value corresponds to CO_2 saturation at about 10 kbar, i.e., a pressure encountered at 35 km below sea level. According to Fig. 6A, the vesicularity predicted by our model at eruption on the oceanic floor (~3300 m) amounts to ~17%, a value in close agreement with that observed (Sarda and Graham, 1990). At depth, when the exsolution of CO_2 takes place, the noble gases initially present in the molten basalt redistribute between vesicles and melt according to Eqs. (10) and (11). The evolution of this partitioning, when magma is rising up, is shown in Fig. 7 as a function of pressure, for bubble formation arising at 35 km under sea level (i.e., 10 kbar). At 5 kbar, helium is equally shared between melt and vesicles (at this pressure $V^* \sim 10^{-2}$, see Fig. 6) while only 35% of neon, 15% of argon and 6% of xenon remain in the melt. At eruption on the seafloor, 96% of the He, 98% of the Ne, 99.6% of the Ar and 99.9% of the Xe atoms are in the vesicles. Furthermore, assuming that the initial $^4He/^{40}Ar$ ratio is about 1.5,

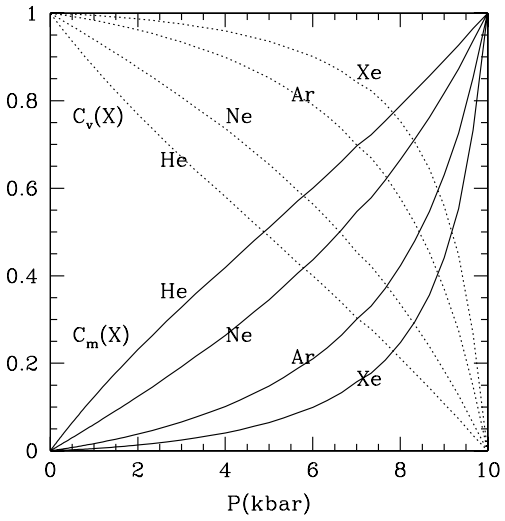

Fig. 7. Concentrations of noble gases in MORB melt (full curves) and in vesicles (dotted curves) during magma ascent when bubble formation starts at 35 km depth (i.e., $P = 10$ kbar) with no loss of vesicles. Concentrations (y-axis) before vesiculation are all taken equal to one for convenience.

as measured in popping rocks (Moreira et al., 1998), our model predicts a concentration ratio around 0.3 in the first vesicles at depth, while, at eruption, this ratio becomes equal to 13.5 in melt and 1.45 in vesicles. Notice that these values agree with noble gas analyses of popping rocks using laser extraction techniques (Burnard et al., 1997), which confirm that popping rocks are undegassed samples of the upper mantle.

Although popping rocks have been the matter of many investigations (Sarda and Graham, 1990; Javoy and Pineau, 1991; Pineau and Javoy, 1994; Burnard et al., 1997; Moreira et al., 1998), the partitioning between vesicles and melt is not known with accuracy, even for these vesicle-rich samples. Crushing basalt glass to analyze the composition of gas escaping from vesicles is a common procedure. By applying successive stages of crushing, one must be able to reach a point where the vesicularity of the crushed sample becomes so small that the residual noble gases are essentially located in melt. An important point for experimentalists is thus to know when this value of vesicularity is reached. Considering a sample of popping rock as a basalt glass issued from the quenching of a melt vesiculated at equilibrium, as described above, it can be easily shown that, after crushing, the elemental ratio in the total sample writes

$$\frac{N_T^i}{N_T^j} = \frac{N_m^i + N_v^i}{N_m^j + N_v^j} = \frac{C_m^i[(1-x) + (\gamma_v^i/\gamma_m^i)x]}{C_m^j[(1-x) + (\gamma_v^j/\gamma_m^j)x]}, \qquad (13)$$

where $N_m^i(N_v^i)$ is the number of noble gas atoms i within the melt (or the vesicles) after crushing, C_m^i is the concentration of noble gas i in melt before crushing (see Eq. (11)) for a glass sample exhibiting a vesicularity V^*, γ_v^i and γ_m^i are the solubility parameters at eruption of the noble gas in vesicles and in melt, respectively, and x is the residual vesicularity of the sample after crushing ($x \ll V^*$). Notice that, when $x = V^*$, the above ratio becomes equal to C_0^i/C_0^j, the initial abundance ratio of the glass sample (e.g., popping rock). As is illustrated in Fig. 8 for a popping rock with $V^* = 0.17$, even in a highly crushed sample (e.g., $x = 10^{-3}$) a majority of xenon atoms are still in the remaining vesicles, while most of the helium atoms are in the melt. Hence, to estimate with accuracy the elemental fractionation N^{He}/N^X (with X = Ne, Ar or Xe) in the melt of a popping rock (by melting the sample residue under vacuum) it is necessary to crush the sample so as to reach a residual vesicularity as small as 10^{-4}–10^{-5} (see Fig. 8), a difficult task for experimentalists.

3.4. Vesicle loss during ascent: usual MORBs

The MORB tholeiites exhibit generally a large variation of vesicularity ($V^* \sim 0.001$–0.17) and elemental fractionation (e.g., He/Ar $\sim$ 1–100). It is well documented that the ratio is negatively correlated with the absolute value of the Ar concentration and with vesicularity as well, and Sarda and Moreira (2002) suggested that a fractionation mechanism at equilibrium between melt and vesicles could account for these trends if one or more stages of vesiculation with partial or total loss of vesicles are involved. In this framework, we have evaluated the noble gas concentrations in melt, in vesicles and in the overall sample, by applying recursively Eqs. (10)–(12) and assuming a

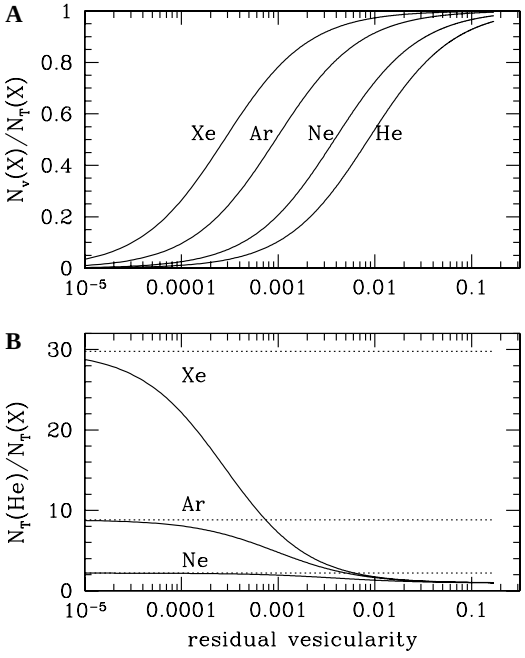

Fig. 8. (A) Fraction of noble gases remaining in the vesicles as function of the residual vesicularity after crushing, for a tholeiite glass with 17% vesicularity erupted 3300 m under sea level (like popping rock 2ΠD43). (B) Evolution, with the residual vesicularity, of the concentration ratio between He and heavier rare gases in the total sample (melt + vesicles) after crushing. The horizontal dotted lines indicate the values of the concentration ratios in melt alone. Initial concentration ratios are taken equal to one.

complete loss of vesicles between two vesiculation events (partial loss may also be implemented). In practice, the initial concentration in melt of species i for vesiculation episode $(n+1)$, $C_0^i(n+1)$, just after episode (n) of vesicle loss, is identified to the concentration $C_m^i(n)$ in melt just before vesicle loss. For illustration, is shown in Fig. 9 the evolution with pressure of the noble gas concentrations in melt and vesicles when the rising magma experiences three vesiculation stages (labelled 1, 2, and 3) ending with total vesicle loss, except the last one. The first vesiculation is assumed to occur at ~35 km below sea level (at this depth $P \sim 10$ kbar and the CO_2 concentration at saturation is around 0.75 wt%, as in a popping rock), a second vesiculation is assumed to occur (for instance) at 16 km (i.e., $P = 4$ kbar) and a third one at 10 km ($P = 2$ kbar). For convenience, the noble gas abundances in melt before vesiculation all are taken equal to 1. By comparing Fig. 9 to Fig. 7, where the MORB experiences only one stage of vesiculation (e.g., popping rock), one can see that the noble gas concentrations in vesicles and their evolution with pressure are greatly affected by the successive stages of vesiculation. In particular, the hierarchy of the noble gas concentrations C_v^i found in vesicles after the first episode of vesicle loss (located at $P = 4$ kbar) is reversed with respect to that observed in the vesicles at the end of the first vesiculation stage. This spectacular effect is caused by the great (weak) amount of light (heavy) atoms remaining in the melt at the end of the first vesiculation stage, and contributes to explain why, in crushing data for natural samples, helium is so abundant when compared to xenon. By contrast, the concentrations C_m^i found in melt exhibit only slight modifications with the successive stages of vesiculation. All these effects are better viewed on the evolution of the $^4He/^{40}Ar$ ratio as a function of the pressure drop accompanying ascent (see Fig. 10), which also clearly illustrates the necessity of vesicle loss (compare to the results of the simple, one-stage, vesiculation history described above). One notices that the closer to the oceanic floor the vesiculation stage, the larger the He/Ar fractionation in melt and in vesicles. Furthermore, at the beginning of the first vesiculation process (10 kbar in the present case) the elemental fractionation in the melt increases rather slowly when magma rises up because of the high density of the fluid phase (CO_2 + rare gases) in vesicles at these depths, which tends to inhibit the transfer of the noble gases from melt to vesicles (see the evolution with pressure of γ_m/γ_g in Fig. 3). This effect is all the more pronounced that vesiculation takes place at a greater depth.

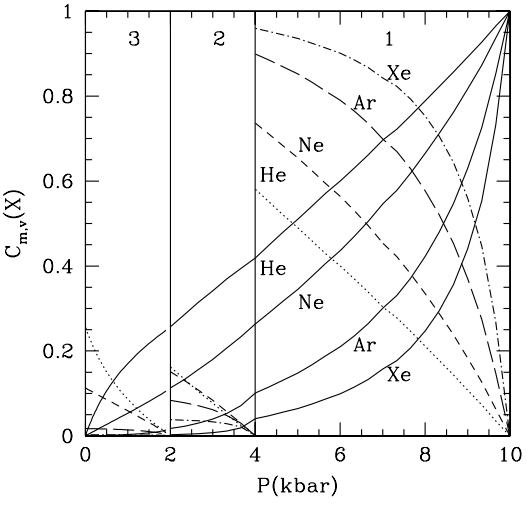

Fig. 9. Evolution with pressure of noble gas concentrations in melt (full curves) and in vesicles for a rising magma exhibiting three stages of vesiculation at 10, 4 and 2 kbar, the vesicles being totally lost at the end of the first and second stages. Initial concentrations before the first vesiculation are all chosen equal to one. Notice that the vesicles become more and more depleted in Ar and Xe with respect to He and Ne with the successive stages during each vesiculation episode.

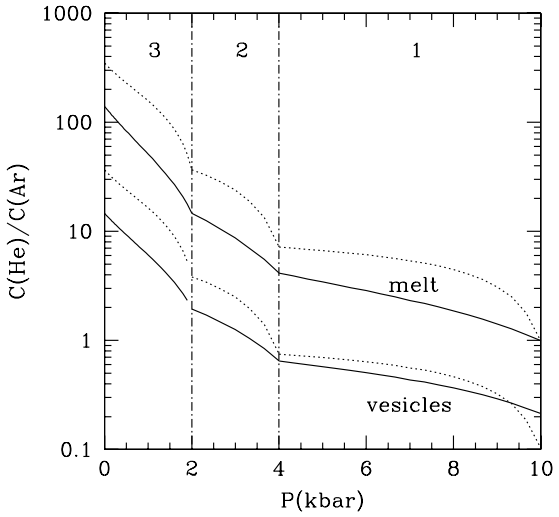

Fig. 10. Evolution of the $^4He/^{40}Ar$ elemental ratio in melt and in vesicles for the rising magma described in Fig. 9. The full curves are the results of the calculations accounting for the variation of the noble gas solubilities with pressure, while the dotted curves are the results obtained assuming Henry's law (see text).

To appreciate the importance of using the correct pressure dependence for solubility parameters γ_m^i and γ_g^i in Eqs. (10) and (11), we also present in Fig. 10 (see dotted curves) the evolution of the elemental fractionation in the framework of the Henry law, i.e., keeping γ_m^i constant and equal to its value at one bar while assuming the gas phase as ideal ($\gamma_g^i = 1$). Clearly, the Henry law overestimates the fractionation both at depth and at eruption, and its use is not recommended when it is question to describe degassing at depth. Moreover, a further scrutiny shows that the deeper the first vesiculation stage in the mantle, the larger the overestimation of the $^4He/^{40}Ar$ ratio at eruption resulting from the use of Henry's law.

As, in our model, the final value of the elemental fractionation, at eruption on the oceanic floor, depends on the number of vesiculation stages and on the depth at which they occur, it is useful to investigate in more details their respective influence. In this framework, the role of a possible disequilibrium of kinetic origin is not accounted for (see Appendix A). In Fig. 11 are presented the values

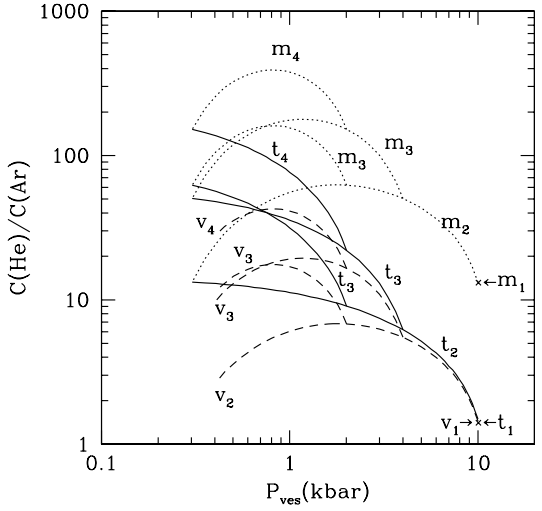

Fig. 11. Variation, with the pressure at which vesiculation starts, of the $^4He/^{40}Ar$ ratio evaluated *at eruption*, 3300 m under sea level, in melt (dotted curves indexed by m_i), in vesicles (dashed curves indexed by v_i) and in the total sample (full curves indexed by t_i) for a representative MORB after $i = 1$, 2, 3, and 4 vesiculation stages with vesicle loss (no vesicle loss for stage 4). Concentrations are normalized to the values found in the popping rock 2Π*D*43 where $C^{He}/C^{Ar} \sim 1.5$ (Moreira et al., 1998). The first vesiculation occurs at $P = 10$ kbar at normal saturation (i.e., 0.75 wt% of CO_2). For example, if the rising magma experiences only one vesiculation stage at $P_{ves} = 10$ kbar, then at eruption the $^4He/^{40}Ar$ ratio in the melt, in the vesicles and in the total sample is given by m_1, v_1 and t_1, respectively. See the text for further explanations.

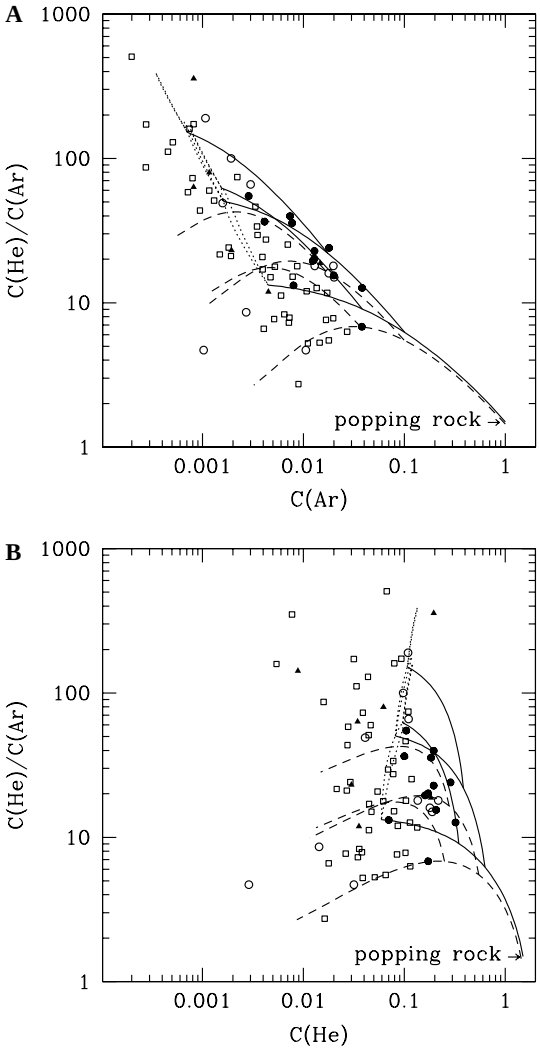

Fig. 12. Variation of the $^4He/^{40}Ar$ ratio *at eruption*, 3300 m under sea level, with the Ar concentration (A), and with the He concentration (B) for a representative MORB after 1, 2, 3, and 4 vesiculations and vesicle loss stages (no vesicle loss for the last stage). As in Fig. 11, values of concentrations are normalized to that found in the popping rock 2Π*D*43 taken as representative of undegassed melt, namely 0.75 wt% of CO_2 and $C^{He}/C^{Ar} \sim 1.5$ with $C^{He} = 8.7 \times 10^{-5}$ cm^3 STP/g (see Moreira et al., 1998). The full curves correspond to the bulk magma (melt + vesicles), the dashed curves to vesicles and the dotted curves to melt, respectively. Full dots (Sarda and Moreira, 2002) and full triangles (Moreira and Allègre, 2002) are data from the literature using step heating and crushing to extract the gas, while empty circles (Aubaud et al., 2004) and empty squares (Burnard et al., 2002, 2004) are data using only crushing. Notice that some uncertainties could affect these data and lead to an underestimation in volatile contents (for example, some helium loss from the native sample is expected and if the crushing is not sufficiently effective a small amount of gas is still remaining in the powder, see Fig. 8). Data showing concentration ratios higher than 100 are likely affected by some kinetic disequilibrium (see Appendix A).

calculated *at eruption* (i.e., for samples collected on the ocean floor at ~3300 m under sea level) of the $^4He/^{40}Ar$ ratio in melt (m), in vesicles (v) and in the overall sample (t) as function of the pressure at which the successive vesiculation stages take place (for illustration, up to four stages are sketched in the figure). The initial abundances in He and Ar are taken close to that exhibited by popping rocks (i.e., $C^{He}/C^{Ar} = 1.5$ with C^{Ar} normalized to 1 for convenience) and the first vesiculation is assumed to occur at ~35 km below sea level ($P_1 = 10$ kbar), i.e., for an initial concentration in CO_2 around 0.75 wt%, similar to that found in popping rocks. The second vesiculation (labelled v_2, m_2, and t_2 in the figure) occurs at various depths between 35 km and the oceanic floor, and two examples of a third vesiculation stage (v_3, m_3, t_3) and one example of a fourth vesiculation (v_4, m_4, t_4) are presented. The shown third vesiculation stages occur between second stage depths of either 13 km (below the oceanic floor, $P_2 = 4$ kbar) or 6 km ($P_2 = 2$ kbar) and eruption. The fourth vesiculation occurs between 6 km ($P_3 = 2$ kbar) and eruption, after a third vesiculation at 6 km (2 kbar), and a second vesiculation at 13 km (4 kbar). As expected, the elemental fractionation is much larger in melt than in vesicles, while it is intermediate in the bulk sample. In general, the fractionation increases with the number of vesiculation stages but astonishingly enough, both in vesicles and in melt, it goes through a maximum value with the pressure of vesiculation. This maximum expresses the variation with pressure of the relative affinity of the rare gases for melt and the CO_2 fluid filling the vesicles: it disappears if solubilities are assumed invariant (Henry's law).

Although it is well established that the $^4He/^{40}Ar$ ratio in MORBs is negatively correlated with the argon concentration (the smaller the concentration, the larger the ratio), the experimental data show a more complex pattern (Honda

and Patterson, 1999; Moreira and Sarda, 2000). Some MORB samples present a relatively low elemental ratio (typically less than 10) associated with a low argon concentration (e.g. in Fig. 12). The important point is that there is not a unique master curve but rather, a large distribution of possibilities. This is precisely what is explained in the framework of our model by the occurrence of different degassing histories. On the other hand, the evolution of the $^4He/^{40}Ar$ ratio with the He concentration and the CO_2 concentration do not show a clear tendency, a feature also well reproduced by the model (see Fig. 12B; the evolution with the CO_2 concentration is not shown because the pattern is very similar to that with He).

Considering the variety of the experimental data (MORB samples dredged from different oceanic ridges and analyzed by different authors), their agreement with the theory is remarkable. It is important to recall that it is the combination of two effects, the multistage vesiculation and the pressure dependence of the solubilities, which is responsible of the heuristicity of the model. If only one continuous vesiculation process was involved during magma ascent, then the distribution of MORB data would be concentrated in only one point in Fig. 12, the one associated with the popping rock. On the other hand, if the variation of the solubilities with pressure at depth was neglected, the multistage vesiculation process would produce essentially a linear arrangement of the data points and not the broad distribution exhibited by the data.

4. Conclusion

We have shown that a simple statistical theory based upon the hard sphere model commonly used in liquid state physics, is able to reproduce and explain noble gas solubility data in compressed silicate melts. In particular, it is pointed out that the concurrent compaction of melt and of the rare gas fluid, in contact with each other, is responsible for the quasi linear variation of the solute concentration with pressure, up to several tens of kbar in some cases. However, this Henry-like behavior is misleading because, on the one hand, the solubility parameter of the noble gas in melt is one or several orders of magnitude lower, in the kbar range and above, than its value at atmospheric pressure and, on the other hand, the rare gas fluid can no longer be considered as ideal because its density is liquid-like in this pressure range. Moreover, at very high pressures, the theory predicts that the noble gas concentration levels off and goes through a maximum value, more or less pronounced depending on the noble gas (e.g., no maximum for helium) and the composition of the silicate melt. The recent high-pressure data of Schmidt and Keppler (2002) on argon and xenon in synthetic haplogranite and tholeiite melts are well reproduced and support our predictions. In contrast, the abrupt drop of argon concentration observed by Chamorro-Perez et al. (1996, 1998) in olivine and in pure silica melts at about 50 kbar seems inconsistent with the previous study and with our model, which instead predicts a gradual decrease of the concentration beyond this pressure range. In this context, we prompt experimentalists to evaluate noble gas solubilities in various liquid silicates around and above the 100 kbar range, and also to investigate the possible influence of noble gas concentrations on the EOS of silicate melts in this pressure range.

Our solubility model is next applied to degassing at mid-ocean ridges. As a consequence of bubble formation at depth induced by the exsolution of CO_2 when magma is rising up, the noble gases divide between melt and vesicles according to their respective solubility in both phases (silicate melt and supercritical fluid CO_2). It is shown that the available experimental data on the pressure dependence of the CO_2 concentration in tholeiitic melts is correctly reproduced by our model. Assuming that the magma starts to vesiculate at approximately 35 km below sea level (i.e., $\sim$10 kbar at saturation in CO_2), and that chemical equilibrium is maintained all along the ascent, the vesicularity evaluated at eruption is found comparable to that observed for the popping rocks ($V^* \sim 0.17$ for $2\Pi D43$). In this case, the model leads to a He/Ar fractionation of 9/1 in melt and 1/1 in vesicles, assuming (for convenience) an initial ratio of 1/1 in the undegassed magma (the estimated concentration ratio for the MORB source mantle is between 1 and 3, Marty and Zimmermann, 1999). However, a simple calculation points out that, to estimate with a reasonable accuracy the He/Ar ratio in melt by heating the powder obtained after crushing, one needs to crush the sample until a residual vesicularity as small as 10^{-4}–10^{-5} is reached. This should be achieved in the future to settle unambiguously if popping rocks are undegassed or partially degassed basalts.

Concerning the usual MORBs, which generally present a large variation of vesicularity and noble gas elemental fractionation, a success of our theoretical approach is to reproduce the trends exhibited by the noble gas concentration and vesicularity data of the literature (data showing obvious signature of kinetic disequilibrium are discarded from the analysis). In this respect, a $^4He/^{40}Ar$ elemental ratio much greater than one in the vesicles is a strong support to the scenario where the rising magma undergoes a series of vesiculation stages at depth interrupted by episodes of vesicle loss. The introduction in the model of the correct pressure dependence for the solubility of noble gases is crucial in this respect. An important consequence of this work is that the elemental fractionation in melt and vesicles keeps the record of the events occurring at depth. This might be an interesting goal for new measurements on MORBs.

Associate editor: Jun-ichi Matsuda

Appendix A

When a very high elemental fractionation is measured in vesicles, i.e., more than $\sim$100 for the He/Ar ratio, this is

likely the signature of a kinetic disequilibrium when vesiculation is taking place at relatively shallow depth. As a matter of fact, the diffusivity of helium in basaltic melts at 1350 °C (Lux, 1987; Watson, 1994) is about 5×10^{-5} cm^2/s, that of argon about 6×10^{-6} cm^2/s and that of CO_2 (solvated as a carbonate ion) about 1×10^{-6} cm^2/s. At about 1100–1200 °C, the temperature of the magma near the ocean floor, the above diffusivities decrease by roughly one order of magnitude, owing to their temperature decay (Watson, 1994). Considering a mean distance between vesicles of about 1 mm (Aubaud et al., 2004; see also Sarda and Graham, 1990), kinetic equilibrium at 1100–1200 °C is reached after about 5 mn for He (the mean square displacement in melt is related to the diffusion coefficient by $r^2 = 6Dt$), 50 mn for Ar and 300 mn for CO_2. For a basaltic melt escaping with a velocity of 2 m/s from a magma chamber located at 6 km below the ocean floor, the eruption takes 50 mn. So, the He concentration in vesicles is at equilibrium and that of Ar is likely not, while CO_2 is certainly not at equilibrium. This simple calculation helps to understand the supersaturation in CO_2 found in some MORB samples (Dixon et al., 1988; Aubaud et al., 2004). In that case, it is also expected that the melt is supersaturated in argon (but to a smaller extent than for CO_2) and hence the argon concentration in vesicles is depleted with respect to its value at equilibrium, a feature which leads to an enhancement of the He/Ar ratio in vesicles (conversely the ratio in the melt becomes lower than expected). For this reason, very high elemental ratios found in vesicles have to be discarded for a proper comparison between our model calculation and experimental data.

References

Agee, C.B., Walker, D., 1988. Static compression and olivine flotation of ultrabasic silicate liquid. *J. Geophys. Res.* **93**, 3437–3449.

Agee, C.B., Walker, D., 1993. Olivine flotation in mantle melt. *Earth Planet. Sci. Lett.* **114**, 315–324.

Andersen, H.C., Weeks, J.D., Chandler, D., 1971. Relationship between the hard-sphere fluid and fluids with realistic repulsive forces. *Phys. Rev.* **A 4**, 1597–1605.

Attard, P., 1993. Simulation of the chemical potential and the cavity free energy of dense hard sphere fluids. *J. Chem. Phys.* **98**, 2225–2231.

Aubaud, C., Pineau, F., Jambon, A., Javoy, M., 2004. Kinetic disequilibrium of C, He Ar and carbon isotopes during degassing of mid-ocean ridge basalts. *Earth Planet. Sci. Lett.* **222**, 391–406.

Boehler, R., Ross, M., Söderlind, P., Boercker, D.B., 2001. High-pressure melting curves of argon, krypton and xenon: deviation from corresponding states theory. *Phys. Rev. Lett.* **86**, 5731–5734.

Bottinga, Y., Javoy, M., 1990. MORB degassing: Bubble growth and ascent. *Chem. Geol.* **81**, 255–270.

Bottinga, Y., Richet, P., Weill, D.F., 1983. Calculation of the density and thermal expansion coefficient of silicate liquids. *Bull. Minéral.* **106**, 129–138.

Burnard, P., 2001. Correction for volatile fractionation in ascending magmas: Noble gas abundances in primary mantle melts. *Geochim. Cosmochim. Acta* **65**, 2605–2614.

Burnard, P., 2004. Diffusive fractionation of noble gases and helium isotopes during mantle melting. *Earth Planet. Sci. Lett.* **220**, 287–295.

Burnard, P., Graham, D., Turner, G., 1997. Vesicle-specific noble gas analyses of "Popping Rock": Implications for primordial noble gases in earth. *Science* **276**, 568–571.

Burnard, P., Graham, D., Farley, K., 2002. Mechanisms of magmatic gas loss along the Southeast Indian Ridge and the Amsterdam-St. Paul Plateau. *Earth Planet. Sci. Lett.* **203**, 131–148.

Burnard, P., Graham, D., Farley, K., 2004. Fractionation of noble gases (He, Ar) during MORB mantle melting: a case study of the Southeast Indian Ridge. *Earth Planet. Sci. Lett.* **227**, 457–472.

Carnahan, N.F., Starling, K.E., 1969. Equation of state for nonattracting rigid spheres. *J. Chem. Phys.* **51**, 635–636.

Carroll, M.R., Draper, D.S., 1994. Noble gases as trace elements in magmatic processes. *Chem. Geol.* **117**, 37–56.

Carroll, M.R., Stolper, E.M., 1991. Argon solubility and diffusion in silica glass: Implications for the solution behaviour of molecular gases. *Geochim. Cosmochim. Acta* **55**, 211–225.

Carroll, M.R., Stolper, E.M., 1993. Noble gas solubilities in silicate melt and glasses: new experimental results for argon and the relationship between solubility and ionic porosity. *Geochim. Cosmochim. Acta* **57**, 5039–5051.

Chamorro-Perez, E., Gillet, P., Jambon, A., 1996. Argon solubility in silicate melts at very high pressures. Experimental set-up and preliminary results for silica and anorthite melts. *Earth Planet. Sci. Lett.* **145**, 97–107.

Chamorro-Perez, E., Gillet, P., Jambon, A., Badro, J., MCMillan, P., 1998. Low argon solubility in silicate melts at high pressure. *Nature* **393**, 352–355.

Dixon, J.E., 1997. Degassing of alkalic basalts. *Am. Mineral.* **82**, 368–378.

Dixon, J.E., Stolper, E., Delaney, J.R., 1988. Infrared spectroscopic measurements of CO_2 and H_2O glasses in the Juan de Fuca Ridge basaltic glasses. *Earth Planet. Sci. Lett.* **90**, 87–104.

Doremus, R.H., 1966. Physical solubility of gases in fused silica. *J. Am. Ceram. Soc.* **49**, 461–462.

Fine, G., Stolper, E., 1985. The speciation of carbon dioxide in sodium aluminosilicate glasses. *Contr. Miner. Petrol.* **91**, 105–121.

Fogel, R.A., Rutherford, M.J., 1990. The solubility of carbon dioxide in rhyolitic melts: A quantitative FTIR study. *Am. Mineral.* **75**, 1311–1326.

Gaetani, G.A., Asimow, P.D., Stolper, E., 1998. Determination of the partial molar volume of SiO_2 in silicate liquids at elevated pressures and temperatures: a new experimental approach. *Geochim. Cosmochim. Acta* **62**, 2499–2508.

Graham, D., 2002. Noble gas isotope geochemistry of mid-ocean ridge and ocean island basalts: Characterization of mantle source reservoirs. *Rev. Mineral. Geochem.* **47**, 247–317.

Graham, D., Sarda, P., 1991. Reply to comment by T.M. Gerlach on "Mid-ocean ridge popping rocks: implications for degassing at ridge crests". *Earth Planet. Sci. Lett.* **105**, 568–573.

Guillot, B., Guissani, Y., 1996a. The solubility of rare gases in fused silica: a numerical evaluation. *J. Chem. Phys.* **105**, 255–270.

Guillot, B., Guissani, Y., 1996b. Towards a theory of coexistence and criticality in real molten salts. *Mol. Phys.* **87**, 37–86.

Hayatsu, A., Waboso, C.E., 1985. The solubility of rare gases in silicate melts and applications for K-Ar dating. *Chem. Geol.* **52**, 97–102.

Hirschfelder, J.O., Curtiss, C.F., Bird, R.B., 1967. *Molecular Theory of Gases and Liquids*, fourth ed. Wiley, New York, p. 1110.

Honda, M., Patterson, D.B., 1999. Systematic elemental fractionation of mantle-derived helium, neon and argon in mid-oceanic ridge glasses. *Geochim. Cosmochim. Acta* **63**, 2863–2874.

Jambon, A., Weber, H., Braun, O., 1986. Solubility of He, Ne, Ar, Kr, Xe in a basalt melt in the range 1250–1600 °C. Geochemical implications. *Geochim. Cosmochim. Acta* **50**, 401–408.

Javoy, M., Pineau, F., 1991. The volatiles record of a "popping" rock from the mid-atlantic ridge at 14 °N: chemical and isotopic composition of gas trapped in the vesicles. *Earth Planet. Sci. Lett.* **107**, 598–611.

Jendrzejewski, N., Trull, T.W., Pineau, F., Javoy, M., 1997. Carbon solubility in Mid-Ocean Ridge basaltic melt at low pressures (250–1950 bar). *Chem. Geol.* **138**, 81–92.

Kirsten, T., 1968. Incorporation of rare gases in solidifying enstatite melts. *J. Geophys. Res.* **73**, 2807–2810.

Kodaka, M., 2001. Reevaluation in interpretation of hydrophobicity by scaled particle theory. *J. Phys. Chem.* **B 105**, 5592–5594.

Lange, R.A., Carmichael, I.S.E., 1987. Densities of Na_2O–K_2O–CaO–MgO–FeO–Fe_2O_3–Al_2O_3–TiO_2–SiO_2 liquids: New measurements and derived partial molar properties. *Geochim. Cosmochim. Acta* **51**, 2931–2946.

Lux, G., 1987. The behaviour of noble gases in silicate liquids: Solution, diffusion, bubbles and surface effects, with applications to natural samples. *Geochim. Cosmochim. Acta* **51**, 1549–1560.

Marty, B., Zimmermann, L., 1999. Volatiles (He, C, N, Ar) in mid-ocean ridge basalts: Assesment of shallow-level fractionation and characterization of source composition. *Geochim. Cosmochim. Acta* **63**, 3619–3633.

Montana, A., Guo, Q., Boettcher, S., White, B.S., Brearley, M., 1993. Xe and Ar in high-pressure silicate liquids. *Am. Mineral.* **78**, 1135–1142.

Moreira, M., Allègre, C., 2002. Rare gas systematics on Mid Atlantic Ridge (37–40 °N). *Earth Planet. Sci. Lett.* **198**, 401–416.

Moreira, M., Sarda, P., 2000. Noble gas constraints on degassing processes. *Earth Planet. Sci. Lett.* **176**, 375–386.

Moreira, M., Kunz, J., Allègre, C.J., 1998. Rare gas systematics in popping rock : isotopic and elemental compositions in the upper mantle. *Science* **279**, 1178–1181.

Pan, V., Holloway, J.R., Hervig, R.L., 1991. The pressure and temperature dependence of carbon dioxide solubility in tholeiitic basalt melts. *Geochim. Cosmochim. Acta* **55**, 1587–1595.

Pierotti, R.A., 1976. A scaled particle theory of aqueous and nonaqueous solutions. *Chem. Rev.* **76**, 717–726.

Pineau, F., Javoy, M., 1994. Strong degassing at ridge crests: The behaviour of dissolved carbon and water in basalt glasses at 14 °N, Mid-Atlantic Ridge. *Earth Planet. Sci. Lett.* **123**, 179–198.

Pitzer, K.S., Sterner, M.S., 1994. Equations of state valid continuously from zero to extreme pressures for H_2O and CO_2. *J. Chem. Phys.* **101**, 3111–3116.

Reiss, H., Frisch, H.L., Helfand, E., Lebowitz, J.L., 1960. Aspects of the statistical thermodynamics of real fluids. *J. Chem. Phys.* **32**, 119–124.

Rigden, S.M., Ahrens, T.J., Stolper, E.M., 1984. Densities of liquid silicates at high pressures. *Science* **226**, 1071–1074.

Rigden, S.M., Ahrens, T.J., Stolper, E.M., 1988. Shock compression of molten silicate: Results for a model basaltic composition. *J. Geophys. Res.* **93**, 367–382.

Sarda, P., Graham, D., 1990. Mid-ocean ridge popping rocks: implications for degassing at ridge crests. *Earth Planet. Sci. Lett.* **97**, 268–289.

Sarda, P., Guillot, B., 2005. Breaking of Henry's law for noble gas and CO_2 solubility in silicate melt under pressure. *Nature* **436**, 95–98.

Sarda, P., Moreira, M., 2002. Vesiculation and vesicle loss in mid-ocean ridge basalt glasses: He, Ne, Ar elemental fractionation and pressure influence. *Geochim. Cosmochim. Acta* **66**, 1449–1458.

Schmidt, B.C., Keppler, H., 2002. Experimental evidence for high noble gas solubilities in silicate melts under mantle pressures. *Earth Planet. Sci. Lett.* **195**, 277–290.

Shibata, T., Takahashi, E., Matsuda, J.-I., 1998. Solubility of neon, argon, krypton and xenon in binary and ternary silicate systems: a new view on noble gas solubility. *Geochim. Cosmochim. Acta* **62**, 1241–1253.

Song, Y., Mason, E.A., 1989. Statistical-mechanical theory of a new analytical equation of state. *J. Chem. Phys.* **91**, 7840–7853.

Tamic, N., Behrens, H., Holtz, F., 2001. The solubility of H_2O and CO_2 in rhyolitic melts in equilibrium with a mixed CO_2–H_2O fluid phase. *Chem. Geol.* **174**, 333–347.

Watson, E.B., 1994. Diffusion in volatile-bearing magmas. *Rev. Mineral.* **30**, 371–409.

White, B.S., Brearley, M., Montana, A., 1989. Solubility of argon in silicate liquid at high pressures. *Am. Mineral.* **74**, 513–529.

Wulf, R., Calas, G., Ramos, A., Büttner, H., Roselieb, K., Rosenhauer, M., 1999. Structural environment of krypton dissolved in vitreous silica. *Am. Mineral.* **84**, 1461–1463.